Deflection and trapping of a counter-rotating vortex pair by a flat plate

Monika Nitsche
Department of Mathematics and Statistics, University of New Mexico, Albuquerque, New Mexico 87131, USA
(Received 22 July 2016; published 28 December 2017; corrected 26 January 2018)

The interaction of a counter-rotating vortex pair (dipole) with a flat plate in its path is studied numerically. The vortices are initially separated by a distance D (dipole size) and placed far upstream of a plate of length L. The plate is centered on the dipole path and inclined relative to it at an incident angle β_i. At first, the plate is held fixed in place. The vortices approach the plate, travel around it, and then leave as a dipole with unchanged velocity but generally a different travel direction, measured by a transmitted angle β_t. For certain plate angles the transmitted angle is highly sensitive to changes in the incident angle. The sensitivity increases as the dipole size decreases relative to the plate length. In fact, for sufficiently small values of D/L, singularities appear: near critical values of β_i, the dipole trajectory undergoes a topological discontinuity under changes of β_i or D/L. The discontinuity is characterized by a jump in the winding number of one vortex around the plate, and in the time that the vortices take to leave the plate. The jumps occur repeatedly in a self-similar, fractal fashion, within a region near the critical values of β_i, showing the existence of incident angles that trap the vortices, which never leave the plate. The number of these trapping regions increases as the parameter D/L decreases, and the dependence of the motion on β_i becomes increasingly complex. The simulations thus show that even in this apparently simple scenario, the inviscid dynamics of a two-point-vortex system interacting with a stationary wall is surprisingly rich. The results are then applied to separate an incoming stream of dipoles by an oscillating plate.

DOI: 10.1103/PhysRevFluids.2.124702

I. INTRODUCTION

The motion of point vortices in otherwise irrotational, inviscid flow is an idealization that gives insight into two-dimensional fluid dynamics. Much research has addressed the dynamics, relative equilibria, and stability of point vortices in unbounded or periodic domains (see Ref. [1] for a review), with new information emerging even for as little as three vortices [2–4]. For simple domains bounded by walls much can be learned by using the classical method of images. Consider a single vortex. In unbounded flow it is stationary and does not move. Near an infinite straight wall it moves parallel to the wall, propelled by image vorticity of opposite sign inside the wall that cancels the normal velocity at the boundary [Fig. 1(a)]. Similarly, a vortex outside of a circular cylinder moves around the cylinder with constant speed [Fig. 1(b)]. If the cylinder is replaced by a flat, finite plate, the vortex rotates around the plate [Fig. 1(c)], with almost constant speed near the two plate sides and faster movement around the edges [Fig. 1(d)]. In all these cases, the closer the vortex is to the wall, the faster it moves. Note that these idealized inviscid solutions neglect viscosity and the associated boundary layer vorticity, which can significantly alter the flow.

Single point vortex motion in more complex domains with solid or moving walls has been studied by using conformal mapping techniques; for example, in Refs. [5–10]. Most closely related to the present work is the study of equilibria of a single vortex near a flat plate performed by Saffman and Sheffield [11] with a view to understanding vortex lift, whereby the equilibria are achieved by adding circulation to the plate. The present paper concerns the study of two vortices in the presence of a wall. Namely, we study the motion of a counter-rotating vortex pair with a flat plate in its path, in otherwise inviscid, irrotational fluid at rest at infinity, by using numerical simulations. We find that even in this apparently simple scenario the revealed vortex dynamics is surprisingly rich.

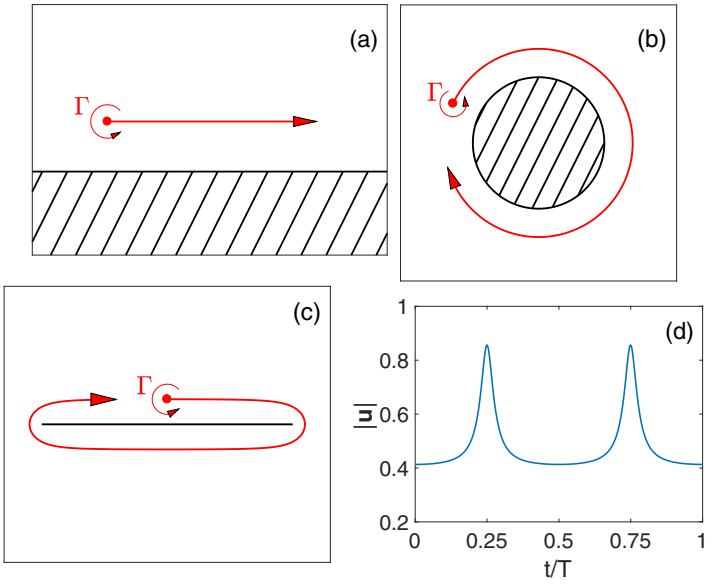

FIG. 1. (a)–(c) Trajectories of single point vortices in simple domains. (d) Speed of vortex in panel (c) vs time t, normalized by the time T required for one rotation. The vortex moves around the plate edges at $t/T = 0.25, 0.75$.

In the absence of the plate, the vortex pair travels as a dipole with constant velocity in direction normal to itself. Dipoles are elementary vortex structures that model, for example, the trailing rolled-up shear layer behind an aircraft, the vortices behind an oar pulled through water, or counter-rotating tidal vortices formed near straits [12]. They occur as robust features in turbulent flows. They play an important part in mixing in the atmosphere and ocean, which led to study their motion on a sphere [13]. Our goal here is to understand the effect of objects in their path. The work builds on that of Archer [14], who studied a more complex system of an elliptically loaded finite vortex sheet [15] interacting with a plate. Archer found that the motion of each vortex sheet half is well approximated by that of point vortices at their centroids, and that the plate, positioned at an angle, can deflect the traveling dipole. This paper presents a more comprehensive study of the reduced point vortex system.

The scenario considered is illustrated in Fig. 2(a). The pair of counter-rotating vortices of strength $\pm\Gamma$, separated by a distance D, is placed above a plate of length L. The vortex pair is placed so far from the plate that it initially travels as a dipole in free space, in the direction normal to itself with constant speed $U = \Gamma/(2\pi D)$. The plate is centered on the dipole path but tilted at an incident angle β_i relative to it. The vortices approach the plate, move around it, and leave as a dipole that quickly reaches the same speed U as it had initially. However, one vortex approaches the plate sooner than the other, and therefore interacts more strongly with the plate, causing the pair to leave at a transmitted angle β_t which is generally different than the incident angle β_i, as illustrated in the example in Fig. 2(b). For certain plate positions the transmitted angle is highly sensitive to changes in β_i. Interestingly, the sensitivity increases as the ratio D/L decreases. In fact, for sufficiently small values of D/L and near critical plate angles the dipole trajectory undergoes abrupt topological changes under infinitesimal changes of β_i or D/L. These singularities occur as discontinuities in the winding number and in the time that the vortices take to move past the plate. The winding number and time delays jump by a finite amount as the plate angle increases across a finite interval, or gap. Within these gaps, further jumps occur repeatedly in a self-similar, fractal fashion. As a result, each gap contains angles with infinite time delays, so that the vortices are trapped and never leave the plate. The number of these trapping regions increases as the parameter D/L decreases,

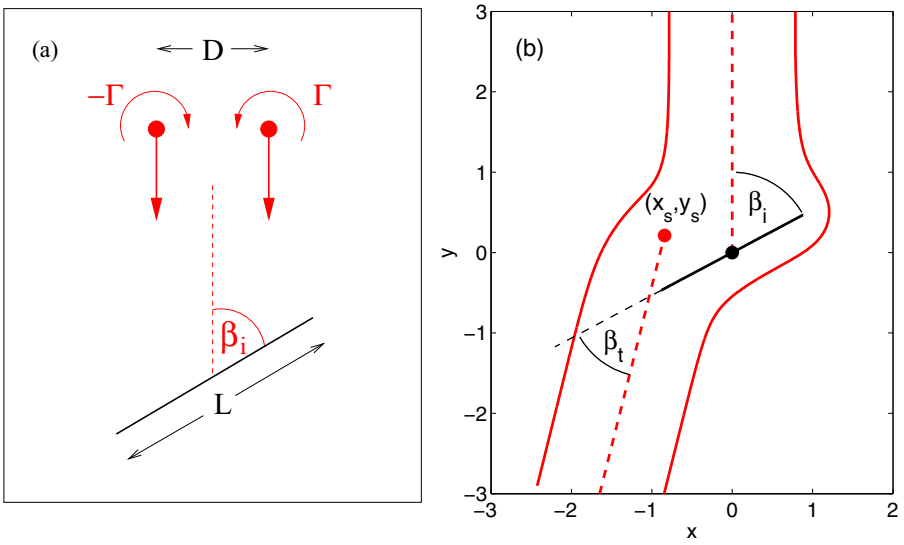

FIG. 2. (a) Sketch showing a dipole consisting of two counter-rotating point vortices with circulation $\pm\Gamma$ separated by a distance D, and a plate of length L centered on the dipole path at an angle. (b) Definition of incident and transmitted angles β_i and β_t, and shift coordinates (x_s, y_s).

and the dependence of the motion on β_i becomes increasingly complex. The observed scattering of the vortex dipoles is reminiscent of the dynamics observed in Ref. [16] for the interaction of pairs of dipoles in unbounded flows.

As a sample application, the sensitive dependence on β_i is used to separate an incoming sequence of dipoles by an oscillating plate. Such a sequence can be thought of as generated by a sequence of airplanes flying one behind another. Each airplane's trailing vortex presents a hazard for following aircraft. The ability to deflect and separate the sequence of vortices could potentially be useful in the airplane vortex wake remediation problem. The present results indicate that, at least in the inviscid idealized point vortex approximation, the incoming dipoles can be separated into an arbitrary number of directions by properly adjusting the plate oscillation period relative to the period at which dipoles enter the domain.

One of the major questions arising in studies of point vortex motion near walls regards the effect of viscosity on the flow. In viscous flow, vorticity generated at the wall separates near edges and interacts strongly with nearby interior fluid vorticity. This effect is not accounted for in the point vortex approximation used here. The inclusion of viscosity in dipole flow past a plate, while out of the scope of this paper, remains an interesting problem to be studied.

The paper is organized as follows: Section II presents the problem considered, the flow nondimensionalization, and the variables used to measure the output. To validate the conclusions of this paper, all results are computed with two different numerical methods. They are described in Sec. III. Section IV presents the numerical results, whereby Sec. IV A presents results for a stationary plate with $D/L = \pi/4$, IV b presents the singular behavior observed within trapping regions for sufficiently small D/L, and Sec. IV C presents the separation of an incoming sequence of vortices by an oscillating plate. Summarizing remarks are made in Sec. V.

II. PROBLEM FORMULATION

The initial configuration is shown in Fig. 2(a). The flow is normalized by the plate half-length $L/2$ and the vortex circulation Γ. That is, if X, Y, T are dimensional coordinates of space and time,

the nondimensional coordinates are

$$x = \frac{X}{L/2}, \quad y = \frac{Y}{L/2}, \quad t = \frac{T}{L^2/(4\Gamma)}. \tag{1}$$

The nondimensional flow parameters for a stationary plate are the incident angle β_i and the relative dipole size D/L. The flow is described in Cartesian coordinates x and y with the origin at the plate center. The point vortices are initially placed at a vertical distance $y_0 = 6$, chosen to be sufficiently large that the reported vortex trajectories remain unchanged to within 0.01% under further increases of y_0. Their initial horizontal coordinate is $\pm x_0 = \pm(D/2)/(L/2) = \pm D/L$. The flow is solely induced by the vortex pair and the presence of the plate. Since any additional external flow is absent, the total circulation around the plate is zero for all times.

The effect of the plate is measured by the transmitted angle β_t of the outgoing dipole trajectory, as defined in Fig. 2(b). The outgoing trajectory is often also shifted away from the plate center. The shift is measured by the coordinates (x_s, y_s) of the point on the outgoing centerline that is closest to the origin. Finally, the time it takes the dipole to move past the plate is measured by the difference τ between t_{12}^p and t_{12}^0, where t_{12}^p is the time from the beginning of the motion a distance of 6 units away from the plate until the vortex pair has again reached a distance of 6 units away from the plate after interacting with it, and t_{12}^0 is the time that the pair would take to traverse the distance of 12 units in the absence of a plate. In other words, τ is the time the dipole is delayed by the plate in traversing a circle of radius 6 centered on the plate. In nondimensional variables,

$$\tau = t_{12}^p - t_{12}^0, \quad t_{12}^0 = \frac{12\frac{L}{2}/U}{L^2/(4\Gamma)} = 48\pi(D/L). \tag{2}$$

If $\tau < 0$ the vortex pair has been accelerated by the plate, if $\tau > 0$ it has been delayed. At a distance bigger than the chosen radius of 6 units, the effect of the plate on the dipole motion is so small that the resulting value of τ remains unchanged to within several digits.

III. NUMERICAL METHOD

The two counter-rotating point vortices are positioned at $\mathbf{x}_{1,2}^v(t)$, with normalized circulation $\Gamma_{1,2} = \pm 1$. They satisfy the initial value problem,

$$\frac{d\mathbf{x}_j^v}{dt} = \mathbf{u}_j(t), \quad j = 1,2, \quad \mathbf{x}_{1,2}(0) = (\pm x_0, y_0), \tag{3}$$

where $x_0 = D/L$, $y_0 = 6$, and $\mathbf{u}_j(t)$ is the velocity of the jth vortex. This system of ordinary differential equations is solved using the fourth-order Runge Kutta method (RK4). The vortex velocity $\mathbf{u}_j$ consists of the flow induced by the other vortex in addition to a potential flow that vanishes at infinity and cancels the normal velocity on the plate. It is found by using two different methods, described next.

A. Method 1: Vortex sheet discretization

Following Ref. [17], the plate is modelled by a vortex sheet in its place whose strength is such that no fluid flows through the plate. The sheet position is given by

$$\mathbf{x}(\alpha,t) = s(\alpha)(\sin\beta_i(t), \cos\beta_i(t)), \tag{4}$$

where $s(\alpha) = \cos(\alpha)$, and $\alpha \in [0,\pi]$. Here, the time dependence of β_i corresponds to plate motions that rotate or oscillate about the center point, as considered in Sec. IV C below. The sheet is discretized by $N+1$ point vortices with position $\mathbf{x}_j(t) = \mathbf{x}(\alpha_j,t)$, $j = 0,\ldots N$, with $\alpha_j = j\Delta\alpha$, $\Delta\alpha = \pi/N$, chosen so that they accumulate at the edges of the plate. Their circulation $\Delta\Gamma_j$ is determined at each time step so that no fluid flows through the plate. The total fluid velocity at a point away from any

point vortex is given by

$$\mathbf{u}(\mathbf{x},t) = \sum_{k=0}^{N} \mathbf{K}(\mathbf{x}-\mathbf{x}_k)\Delta\Gamma_k + \sum_{k=1}^{2} \mathbf{K}\big(\mathbf{x}-\mathbf{x}_k^v\big)\Gamma_k, \tag{5}$$

where $\mathbf{K}(\mathbf{x}) = \frac{1}{2\pi}(-y,x)/(x^2+y^2)$, $\mathbf{x} = (x,y) \neq \mathbf{0}$. The no-through-flow condition is imposed at the midpoints between the vortices $\mathbf{x}_j^m(t) = \mathbf{x}((\alpha_j + \alpha_{j+1})/2,t)$,

$$(\mathbf{u}\cdot\mathbf{n})\big(\mathbf{x}_j^m,t\big) = (\mathbf{U}_p\cdot\mathbf{n})\big(\mathbf{x}_j^m,t\big), \quad j = 0,\ldots,N-1, \tag{6a}$$

where $\mathbf{U}_p$ is the prescribed plate velocity at $\mathbf{x}^m$ at time t, and $\mathbf{n}$ is a unit vector normal to the plate at time t. Note that $\mathbf{U}_p$ is nonzero only in the oscillating-plate-case considered in Sec. IV C. These N conditions (6a) are supplemented by zero total circulation,

$$\sum_{k=0}^{N} \Delta\Gamma_k = 0. \tag{6b}$$

Equations (6a) and (6b) form a linear system that determines the $N+1$ values of $\Delta\Gamma_k$ at each time. The coefficient matrix is time independent and can be factored initially, so that only two triangular solvers are needed to find $\Delta\Gamma_k$ at each stage of the time-stepping scheme. This procedure determines the time-dependent vortex sheet strength on the plate; that is, the image vorticity necessary to satisfy the no-penetration condition. The resulting velocity of the jth vortex is

$$\mathbf{u}_j(t) = \sum_{k=0}^{N} \mathbf{K}\big(\mathbf{x}_j^v-\mathbf{x}_k\big)\Delta\Gamma_k + \sum_{\substack{k=1\\k\neq j}}^{2} \mathbf{K}\big(\mathbf{x}_j^v-\mathbf{x}_k\big)\Gamma_k. \tag{7}$$

B. Method 2: Conformal mapping technique

Alternatively, one can apply the Routh rule to find the vortex velocity ([1], §3.3): the region outside the plate is mapped conformally to the region outside a cylinder, the complex velocity potential in the mapped plane is obtained by using images, and the point vortex velocity in the original plane is deduced from it. This method has been applied to compute single point vortex flow around a plate [11] or in more complex domains [5–9] as well as symmetric two-point-vortex flow with steady or moving boundaries [10,18]. The related Hamiltonian theory is well covered in Saffman's monograph [18]. For any system of N point vortices, the Hamiltonian is a function that is conserved along particle trajectories. In the single and symmetric two-point vortex flows referred to above, the Hamiltonian reduces to a function of two variables whose level curves yield the vortex trajectories without requiring integration in time. In the present work, in which there is no imposed symmetry, the Hamiltonian is a function of four variables, and the trajectories are obtained by numerical integration. Below, we evaluate the Hamiltonian of the computed trajectories to determine the accuracy of the simulation.

The conformal map used here (see Fig. 3) is given by

$$\zeta = f(z) = e^{i\beta}z + \sqrt{e^{2i\beta}z^2+1}, \tag{8}$$

where $\beta = \beta_i$, using appropriate branch cuts for the square root. The point vortices are mapped to $\zeta_{1,2} = f(z_{1,2})$. The point vortex velocity $\mathbf{u}_j(t)$ is obtained by using the Routh rule, which we briefly derive here for the case of a fixed plate in which β is constant, closely following the description in Newton ([1], §3.3). First, the velocity potential in the ζ plane at a point $\zeta \neq \zeta_1,\zeta_2$ is obtained by using image vorticity in the cylinder,

$$W(\zeta) = W_0^j(\zeta) + \frac{\Gamma_j}{2\pi i}\log(\zeta-\zeta_j), \tag{9a}$$

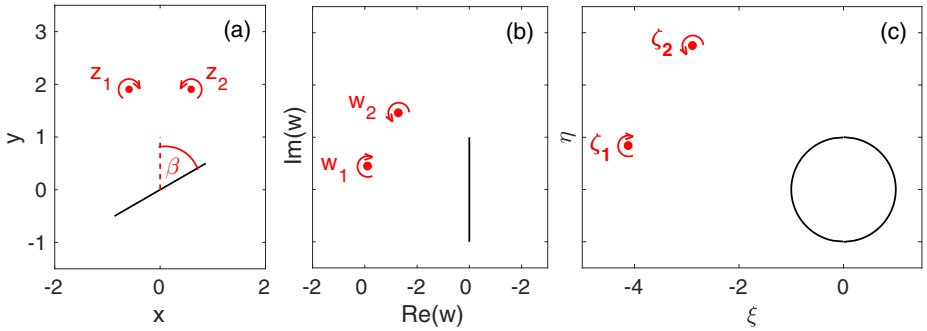

FIG. 3. Conformal map $\zeta = f(z)$ from outside the plate to outside the cylinder. (a) Point vortices $z_k = x_k + iy_k$ and plate in the z plane. (b) Rotation into the w plane, $w = e^{i\beta}z$. (c) Map to the ζ plane, $\zeta = w + (w^2+1)^{1/2}$.

where

$$W_0^j(\zeta) = \sum_{\substack{k=1\\k\neq j}}^{2} \frac{\Gamma_k}{2\pi i}\log(\zeta-\zeta_k) - \sum_{k=1}^{2}\frac{\Gamma_k}{2\pi i}\log\left(\zeta - \frac{\zeta_k}{|\zeta_k|^2}\right) \tag{9b}$$

contains all contributions except that of the jth vortex. The velocity in the z plane at a point $z \neq z_j$ is given by the complex velocity $W'(f(z))f'(z)$. The velocity at z_j is then obtained by taking the limit of the complex velocity as $z \to z_j$, after removing the self-induced velocity of z_j,

$$\begin{aligned}(u_j - iv_j)(t) &= \left(W_0^j\right)'(f(z_j))f'(z_j) + \frac{\Gamma_j}{2\pi i}\lim_{z\to z_j}\left[\frac{f'(z)}{f(z)-f(z_j)} - \frac{1}{z-z_j}\right]\\ &= \left(W_0^j\right)'(f(z_j))f'(z_j) + \frac{\Gamma_j}{4\pi i}\frac{f''(z_j)}{f'(z_j)}.\end{aligned} \tag{10}$$

The corresponding Hamiltonian function is (see Ref. [1], §3.6)

$$H(z_1,z_2) = -\frac{1}{4\pi}\sum_{j=1}^{2}\Gamma_j^2\log\frac{|f'(z_j)|}{|1-f_j\overline{f_j}|} - \frac{1}{4\pi}\sum_{j=1}^{2}\sum_{\substack{k=1\\k\neq j}}^{2}\Gamma_j\Gamma_k\log\frac{|f_j-f_k|}{|1-f_j\overline{f_k}|}, \tag{11}$$

where $f_j = f(z_j)$ and the overline denotes complex conjugation.

Equations (7) and (10) give the velocity $\mathbf{u}_j(t)$ by using methods 1 and 2, respectively. Method 1 is more general than method 2 since it does not require a conformal map and is not bound to planar geometries. For example, it is easily applicable to complex geometries or axisymmetric flows. Method 2 returns the exact velocity without dependence on a spatial discretization parameter N and is significantly faster. To validate in particular the highly singular results shown below, all results in Secs. IV A and IV B are computed with both methods. For the regular flows displayed in Figs. 4–6, the two methods, using $N = 80$ and $0.005 \leqslant \Delta t \leqslant 0.05$, agree to within more than seven digits and are indistinguishable at the scales shown. For the singular behavior displayed in Figs. 6–10, most results, computed with $N = 160$ and $0.002 \leqslant \Delta t \leqslant 0.005$, agree to within more than five digits. The results with method 1 are shown to converge to those of method 2 as $N \to \infty$, $\Delta t \to 0$. The regular flows with oscillating plate motion in Sec. IV C are computed with method 1.

IV. RESULTS

A. Deflection by a stationary plate, for $D/L = \pi/4$

This section presents the dipole trajectory in the presence of a stationary plate, with fixed dipole size $D/L = \pi/4$. This particular value corresponds to a pair of vortices at the centroids of

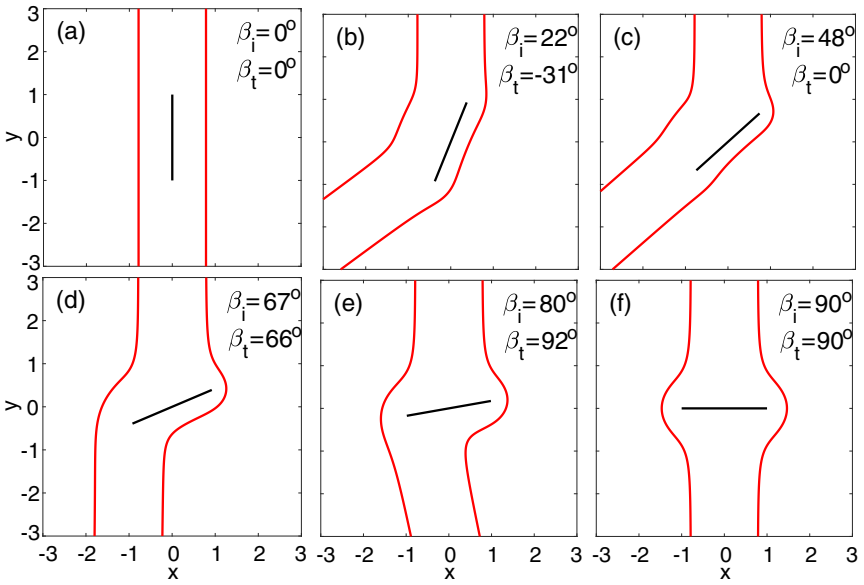

FIG. 4. Vortex trajectories for $D/L = \pi/4$ and (a) $\beta_i = 0°$, (b) 22°, (c) 48°, (d) 67°, (e) 80°, (f) 90°.

an elliptically loaded vortex sheet of length L. Figures 4(a)–4(f) show the trajectories for various incident angles β_i, as indicated. After interacting with the plate, the dipole leaves with the transmitted angle β_t, also indicated in each figure. Note that, in all cases shown in this paper, the final dipole velocity and vortex separation is within 0.01% of the initial one. This difference can be made arbitrarily small by increasing the initial and final distance of the vortices from the plate. That is, in the limit as $t \to \pm\infty$, when the influence of the plate vanishes, the vortex velocity and dipole size are identical.

In Fig. 4(a), the plate is parallel to the incoming dipole trajectory; that is, $\beta_i = 0°$. It is aligned with a streamline of the flow induced solely by the dipole, which therefore satisfies the no-penetration condition. No additional image vorticity is generated on the plate and the dipole travels undisturbed, as if the plate were absent, with $\beta_t = \beta_i = 0°$.

In Fig. 4(b), the plate is slightly inclined, with $\beta_i = 22°$. The dipole is deflected to the left and leaves with negative transmitted angle $\beta_t \approx -31°$. To better understand the deflection, note that, as the dipole travels downwards, the right vortex approaches the plate more closely than the left vortex. Because of its positive circulation, it moves clockwise propelled by the opposite-signed vorticity in the wall, to the other side of the plate. At that time the effect of each vortex on the other is reduced, so that each travels mainly in the image vorticity field of the plate, parallel to it. The right vortex is closer and travels faster. As a result, after pairing up again at the other end of the plate, the relative position of the vortices has changed and they leave at a different angle.

In Fig. 4(c), the plate is inclined further, with $\beta_i = 48°$. In this case, the dipole is also deflected to the left, but leaves the plate almost parallel to it, with $\beta_t \approx 0°$. In Fig. 4(d), with $\beta_i = 67°$, the dipole direction is almost unchanged by the interaction; that is, $\beta_t \approx \beta_i$. However, the path is clearly shifted to the left. In Fig. 4(e), with $\beta_i = 80°$, the dipole is deflected to the right, with $\beta_t \approx 92° > \beta_i$. In Fig. 4(f), the dipole approaches the plate normal to it, each vortex surrounds the plate symmetrically, and the dipole leaves on the other side normal to the plate, with $\beta_t = \beta_i = 90°$.

Figure 5 summarizes the flow past the stationary plate for all $\beta_i \in [0,90]$, for the case $D/L = \pi/4$. Figure 5(a) plots the transmitted angle β_t as a function of β_i. There are three points on the graph, denoted by a, d, and f, at which the transmitted angle equals the incident angle, $\beta_t = \beta_i$. These points, with $\beta_i = 0°, 67°, 90°$, correspond to the three trajectories shown in Figs. 4(a), 4(d), and

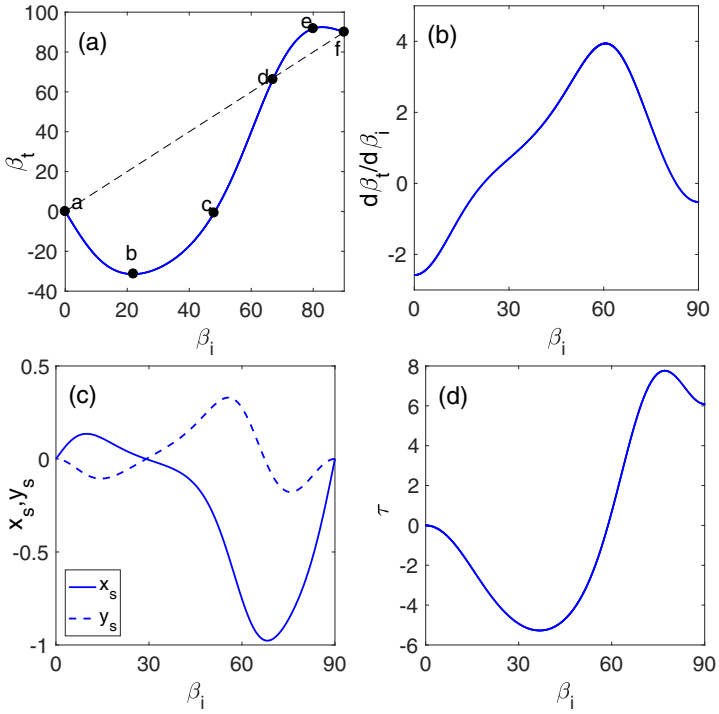

FIG. 5. (a) Transmitted angle β_t, (b) derivative $d\beta_t/d\beta_i$, (c) trajectory shift coordinates x_s and y_s, and (d) time delay τ, vs β_i, for $D/L = \pi/4$. The solid dots in panel (a) denote the pairs (β_i, β_t) plotted in Fig. 4.

4(f). For $0 < \beta_i < 67^\circ$, the dipole is deflected to the left, with $\beta_t < \beta_i$. For $67^\circ < \beta_i < 90^\circ$, the dipole is deflected to the right, with $\beta_t > \beta_i$. Points b and e denote those at which the deflection to the left and right is close to maximal, and correspond to the trajectories shown in Figs. 4(b) and 4(e). Points a and c are the only points at which the dipole leaves the plate parallel to it, with $\beta_t = 0^\circ$, and correspond to the trajectories shown in Figs. 4(a) and 4(c). Figure 5(b) plots the derivative $d\beta_t/d\beta_i$ vs β_i. The derivative measures the sensitivity of the transmitted angle to changes in the incident angle; that is, the change in β_t per change in β_i. The figure shows that the transmitted angle is most sensitive to changes in the incident angle for $\beta_i \approx 60^\circ$.

Figure 5(c) shows the shift of the outgoing trajectory, measured by the coordinates (x_s, y_s) defined in Fig. 2(b). The most notable feature is the large minimum value of x_s near $\beta_i = 67^\circ$, reflecting the leftward shift of the outgoing dipole trajectory by about half the plate length seen in Fig. 4(d). The dipole trajectory is never shifted by more than half the plate length.

Figure 5(d) plots the time delay τ of the dipole caused by the interaction with the plate. As explained, it measures the additional time it takes to approach and leave the plate by 6 units in the presence of the plate as compared to without the plate. The distance of 6 units is chosen to be so large that the time delay τ remains unchanged by further increasing it. The figure shows that for $0^\circ < \beta_i < 60^\circ$, the dipole is accelerated by the plate, with $\tau < 0$. For $60^\circ < \beta_i \leqslant 90^\circ$, the presence of the plate slows the dipole down, with $\tau > 0$. To put these values into perspective, note that, absent the plate, the dipole would traverse one plate length in time $8\pi(D/L)$. So, for $D/L = \pi/4$, the maximal delay of $\tau \approx 8$ represents about 40% of that time.

B. Dipole trapping for $D/L < 0.471\pi/4$

Section IV A presented results for one value of $D/L = \pi/4$. This section addresses the effect of decreasing D/L, corresponding to either smaller dipoles or larger plates. As before, the plate is

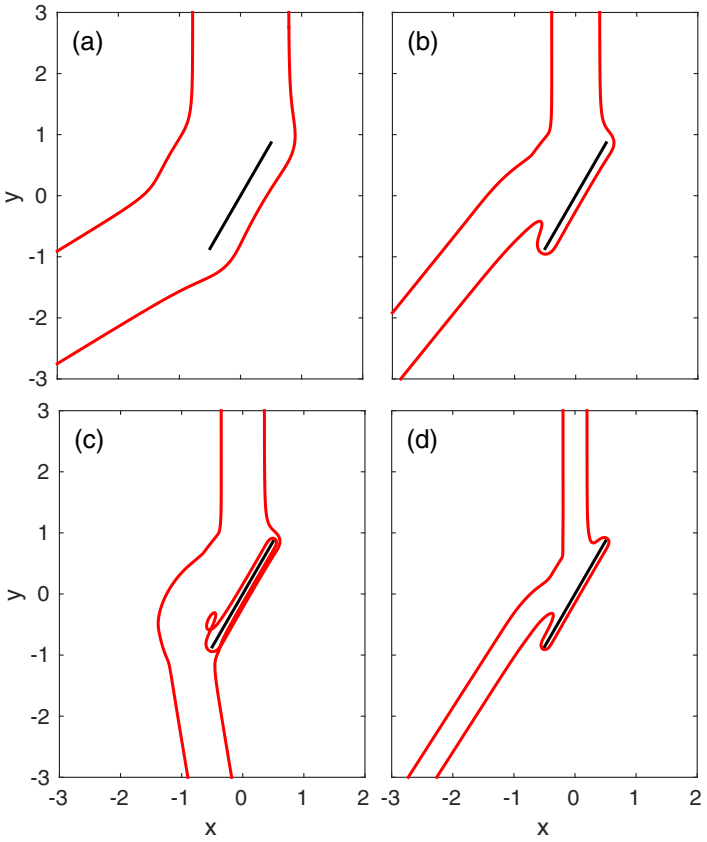

FIG. 6. Vortex trajectories for $\beta_i = 30^\circ$ and (a) $D/L = \pi/4$, (b) $0.5\pi/4$, (c) $0.45\pi/4$, (d) $0.25\pi/4$.

stationary throughout. Figure 6 plots trajectories for incident angle $\beta_i = 30^\circ$ and decreasing values of $D/L = \pi/4, 0.5\pi/4, 0.45\pi/4, 0.25\pi/4$. As D/L decreases, the right vortex approaches the plate more closely. Its motion is thus increasingly dominated by the plate, so that it behaves more closely to a single vortex near a plate. As noted earlier, a single vortex would rotate indefinitely around the plate, with larger speeds the closer it is to it. This behavior is described in more detail in the appendix. Meanwhile, the left vortex, which is further away, moves slowly along the plate. In all four cases, the two vortices eventually pair up again and leave the plate as a dipole, with constant direction and velocity.

However, an interesting feature occurs as D/L decreases from $0.5\pi/4$ in Fig. 6(b) to $0.45\pi/4$ in Fig. 6(c). Note that in Fig. 6(b), after turning around the left plate corner, the right vortex pairs up with the left vortex, *backs up*, and both leave the plate as a dipole. In Fig. 6(c) on the other hand, as can be seen in the closeup in Fig. 7, the right vortex completely circles the plate and *never unwinds* before pairing up with the left vortex and leaving the plate. Thus the winding number, the number of turns the vortex makes about the plate before leaving, of the right vortex has increased by one between Fig. 6(b) and Fig. 6(c), while the winding number of the left vortex has remained unchanged at zero. There is therefore no continuous transformation from paths of the form of 6(b) to paths of the form of 6(c), and thus the dipole paths, as a function of D/L, have to break and suffer a topological discontinuity between these two values of D/L. That is, if the vortex trajectories were replaced by rubber bands held together at the beginning and end, the right band would have to be cut and reattached to transition from shape 6(b) to shape 6(c). The discontinuity, characterized here by a jump in the winding number, is studied in more detail below. Another such discontinuity occurs

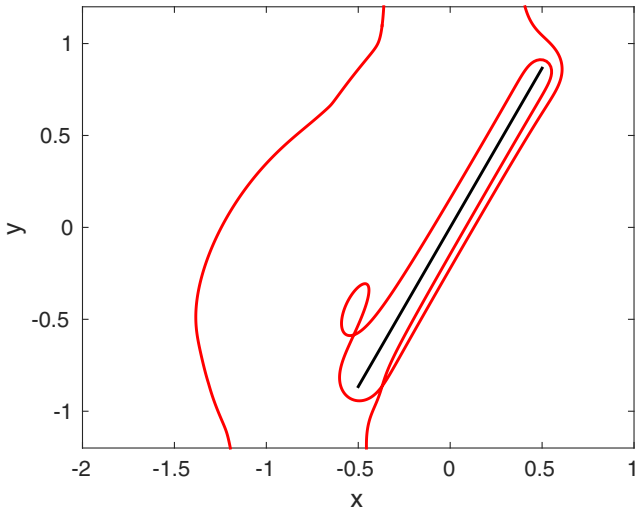

FIG. 7. Closeup of figure 6(c).

between $D/L = 0.45\pi/4$ in Fig. 6(c) and $D/L = 0.25\pi/4$ in Fig. 6(d), since in Fig. 6(d) the right vortex clearly backs up again to leave the plate with zero winding number.

The results in Figs. 6 and 7 were computed with both methods described in Sec. III by using equal time steps $\Delta t = 0.005$, with identical results to within more than seven digits. To confirm the accuracy of the integration in time using RK4, Fig. 8 shows the extent to which the computed Hamiltonian $H(t)$ departs from its initial value, for the case in Fig. 7. Figure 8(a) plots the difference $|H(t) - H_0|$, where $H_0 = H(0)$, computed with the indicated values of Δt. It shows that $H(t)$ is almost constant, with errors that decrease as Δt decreases. Figure 8(b) plots the maximal error as a function of Δt, and shows that it decreases as Δt^3. The slightly less than optimal convergence for

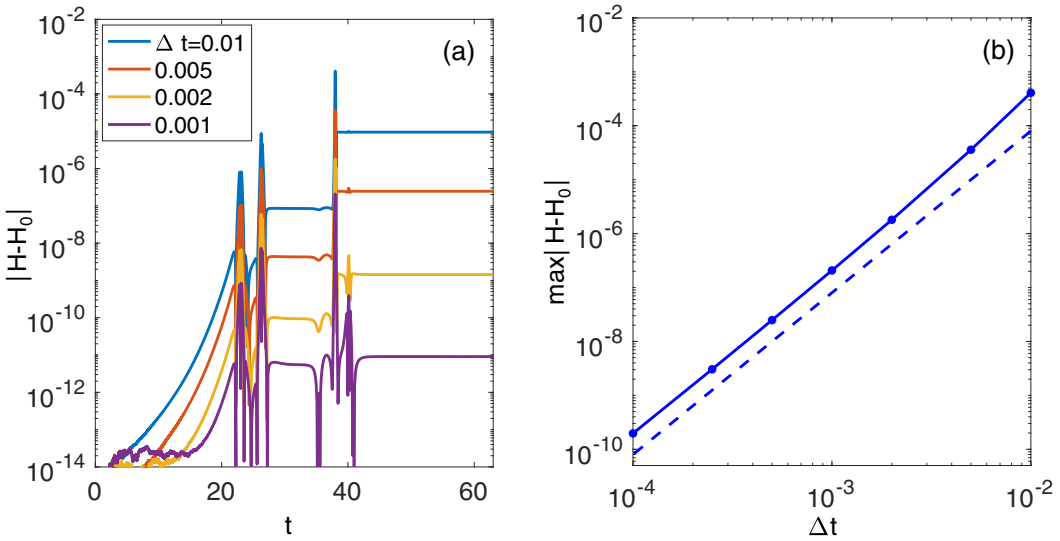

FIG. 8. Hamiltonian $H(t)$ for $\beta_i = 30^\circ$ and $D/L = 0.45\pi/4$. (a) $|H(t) - H_0|$ vs t, where $H_0 = H(0)$, computed with the indicated values of Δt. (b) $\max_{t\in[0,60]} |H(t) - H_0|$ vs Δt. The dashed line has slope three.

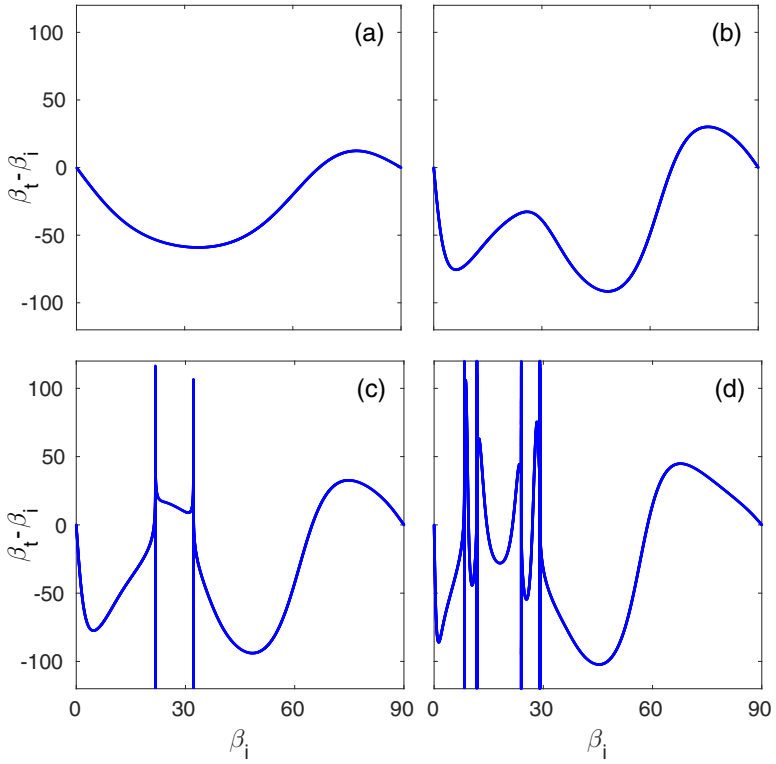

FIG. 9. Transmitted angle $\beta_t - \beta_i$ vs β_i, for (a) $D/L = \pi/4$, (b) $0.5\pi/4$, (c) $0.45\pi/4$, and (d) $0.25\pi/4$.

RK4 is attributed to the fact that the computed problem is stiff: small changes in the initial condition lead to large changes in the outgoing trajectories. Nonetheless, Fig. 8 shows that the trajectory shown in Fig. 7, computed with $\Delta t = 0.005$, is a highly accurate solution to the point vortex equations.

Figure 6 showed results for various values of D/L, but only one incident angle β_i. We now present the dependence on β_i as well as D/L. Figure 9 shows the transmitted angle β_t as a function of β_i, for $\beta_i \in [0,90]$ and the same four values of D/L as in Fig. 6. It plots the difference $\beta_t - \beta_i$. For $D/L = \pi/4$ this difference was shown in Fig. 5(a) to have three roots. Figure 9 shows that, as D/L decreases, the number of roots increases, as does the derivative $d\beta_t/d\beta_i$; that is, the sensitivity of the transmitted angle with respect to changes in the incident angle. More strikingly, though, is that for the two smallest values of D/L in Figs. 9(c) and 9(d), the transmitted angle has highly singular behavior in at least two regions in Fig. 9(c), and four regions in Fig. 9(d). In these regions β_t oscillates rapidly between -180° and 180°. These rapid oscillations occur over an interval in β_i. Plots of the corresponding dipole trajectories show that as β_i changes across these intervals, the trajectories undergo a topological discontinuity as observed before under changes in D/L (Fig. 6). That is, the discontinuities occur near critical angles for sufficiently small D/L if either D/L or β_i is changed.

To more accurately describe the singular events observed, we compute the winding number α of the right vortex, defined as follows: as the vortex, positioned at the point $X(t) = \mathbf{x}_2(t)$, moves, the vector $\overline{OX}(t)$ subtends an angle $\tilde{\alpha}(t)$ with the positive y axis. Since the particle motion is continuous, the angle $\tilde{\alpha}$ increases or decreases continuously. Each time the particle surrounds the plate, and thus the origin, in the clockwise direction, $\tilde{\alpha}$ increases by 2π. We define the winding number $\alpha = \lim_{t\to\infty} \tilde{\alpha}(t)/(2\pi)$. With this definition the winding number of the right vortex in Fig. 6(b) is approximately 0.6, while in Fig. 6(c) it is approximately 1.45.

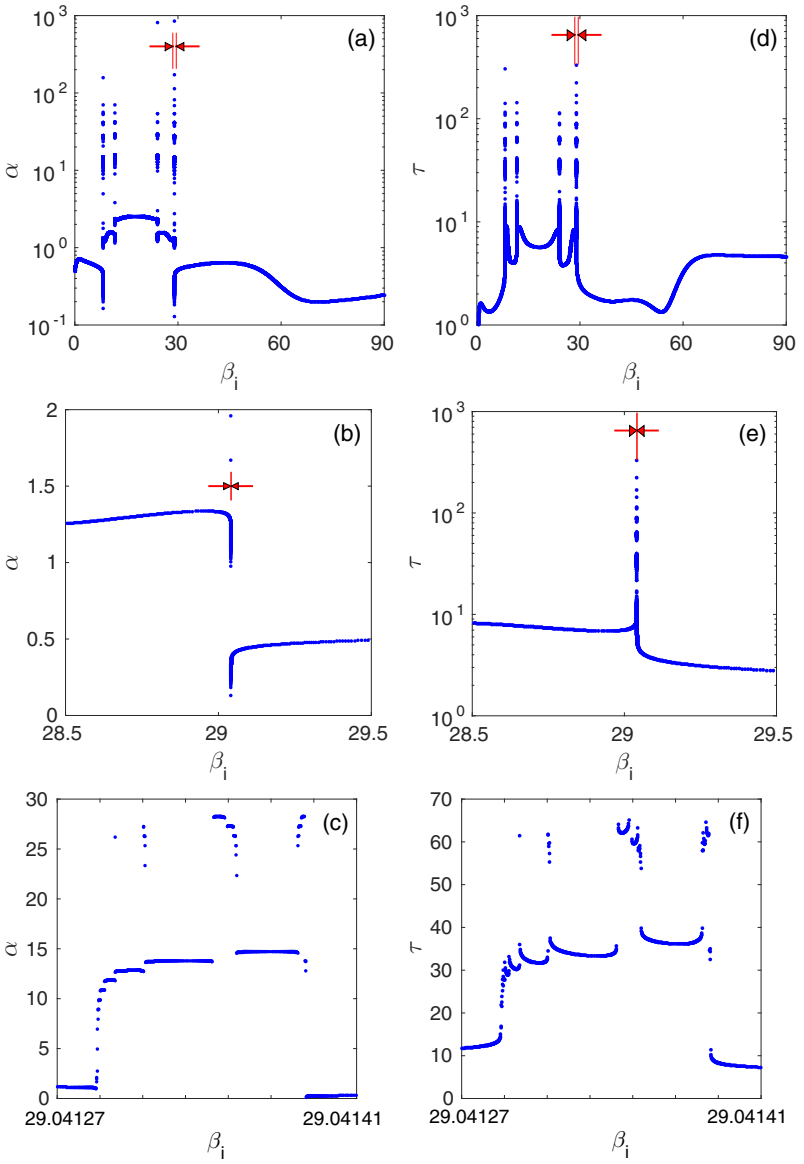

FIG. 10. Singular behavior for $D/L = 0.25\pi/4$, computed with conformal mapping technique (method 2) with $\Delta t = 0.0002$. (a)–(c) Winding number α vs β_i, at three different scales. (d)–(f) Time delay τ vs β_i, at three different scales.

Figure 10(a) plots the winding number α as a function of β_i, for $\beta_i \in [0,90]$ and $D/L = 0.25\pi/4$, on a logarithmic scale. The values of β_i are sampled in steps as small as 10^{-9}. Four intervals are visible in which α is discontinuous. These intervals correspond to those in Fig. 9(d) in which β_t is singular. Remarkably, not only does α jump across these intervals, but within each of them there are many angles for which the winding number is extremely large, as large as 1000. Figure 10(b) shows a closeup of the region in Fig. 10(a) near $\beta_i = 29$, of width as indicated by the red arrows in Fig. 10(a). It shows, on a linear scale, that α decreases by one across the interval, jumping down from one continuous branch of values to another. However, much structure is contained between

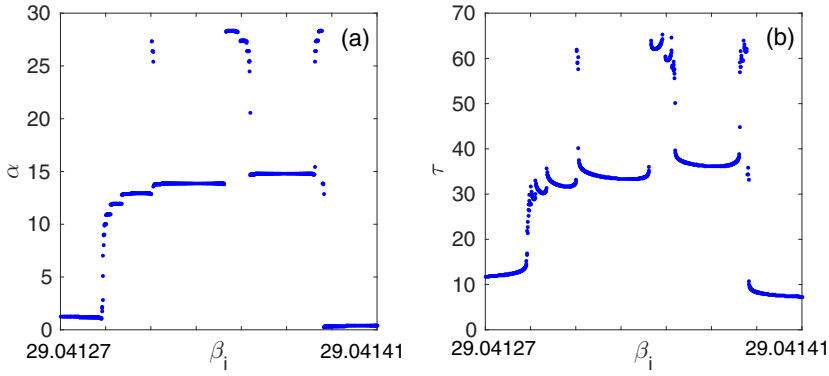

FIG. 11. Winding number and time delay τ computed with vortex sheet discretization (method 1), using $N = 160$, $\Delta t = 0.0002$, for D/L and β_i as in Figs. 10(c) and 10(f).

these two branches. Figure 10(c) shows a closeup of the region in Fig. 10(b) of width as indicated by the red arrows in Fig. 10(b). It shows that the jump seen in Fig. 10(b) occurs over a finite gap of width approximately 0.0001. This gap, in turn, contains many jumps across gaps to other continuous branches. Indeed, each of these smaller gaps appears to contain more jumps to further continuous branches across gaps. The results indicate the presence of gaps within gaps within gaps, across each of which the winding number jumps by one between continuous branches, in a fractal fashion. Although limited numerically by finite resolution and accuracy, more detail to the fractal nature is given in Fig. 13 below.

Figures 10(d)–10(f) plot the time delay τ that the vortices require to traverse the plate, for the same values of β_i shown in Figs. 10(a)–10(c). It shows that the time delays are proportional to the winding numbers. Each gap across which α jumps not only contains large winding numbers close to 1000, but also large time delays. As seen by comparing Figs. 10(c) and 10(f), each jump in α corresponds to a jump in τ from one continuous branch to another across a gap, and each of these gaps contains more continuous branches with gaps across which τ jumps.

To validate this highly singular, unexpected behavior in a simple two-point vortex flow, we remind the reader that all results in Secs. IV A and IV B were computed with the two different methods described in Sec. III. For all results shown in Figs. 4–9, the two methods agree to within seven or more digits, and are indistinguishable at the scales shown. Most winding numbers and time delays shown in Fig. 10 agree to within five or more digits. Figure 11 more clearly visualizes the agreement between the two methods. While Fig. 10 shows the values of α,τ computed with the accurate conformal mapping technique (method 2), using $\Delta t = 0.0002$, Fig. 11 shows the same quantities but computed with the vortex sheet discretization (method 1), using $N = 160$ and $\Delta t = 0.0002$. There are only a handful of points in Fig. 11 within the highly singular gaps that visibly differ from those in Fig. 10. Pointwise convergence of method 1 to method 2 as $N \to \infty$, $\Delta t \to 0$, is shown in Fig. 12, for a value of $\beta_i = 29.041\,33$ within the gap seen in Fig. 10(c) for which the winding number is $\alpha = 15$. The figure plots the norm of the difference between the two methods in the vortex position at $t = 60$, after the right vortex has circled the plate 15 times and the pair has left the plate, computed with a range of values of N and Δt. It shows that the difference decreases fast, approximately as $(1/N)^{10}$, until it reaches either the time-stepping error, or roundoff error. Roundoff error is relatively large due to the large number of time steps taken, and the stiffness of the problem. The agreement between two quite distinct numerical methods, shown in Figs. 10–12, in addition to the conservation of the Hamiltonian shown in Fig. 8, validates the highly singular fractal dependence of the vortex trajectories on β_i that is observed. Furthermore, the fact that one method has more error than the other, yet gives almost identical results, shows that the results are not sensitive to details of the numerical method, thus demonstrating numerical robustness of the observed behavior.

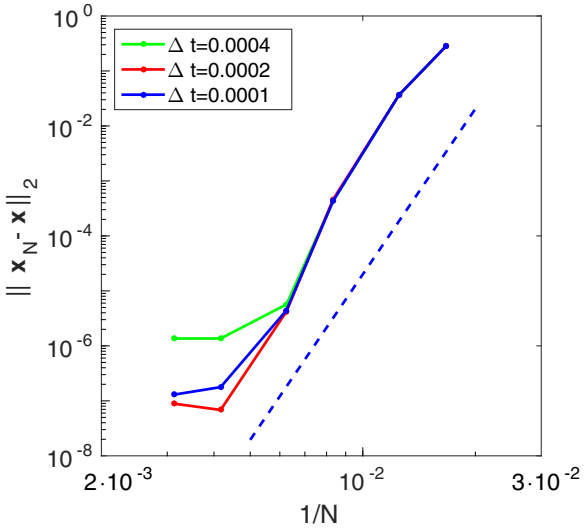

FIG. 12. Convergence of vortex pair position for $D/L = 0.25\pi/4$, $\beta = 29.04133$, at $t = 60$. The point coordinates $\mathbf{x}_N$ are those computed with method 1 with $N = 60, 80, 120, 160, 240, 330$. The point coordinates $\mathbf{x}$ are those computed with method 2. The values of Δt are as indicated. The dashed line has slope ten.

The complexity of the dependence of the vortex trajectories on β_i increases as D/L decreases. Figure 13 plots the winding number α for a smaller value of $D/L = 0.167\pi/4$ than in Fig. 10. At the coarsest level, in Fig. 13(a), six gaps are visible across which α jumps by one. As in Fig. 10, each of these gaps contains continuous branches with gaps, at infinitum. However, in addition, Fig. 13 shows another feature. A closeup of the region near the leftmost gap whose width is indicated by the red arrows in Fig. 13(a) is shown in Fig. 13(b). It shows the presence of another gap, not within the original gap at $\beta = 5.08$, but near it, around $\beta = 5.16$. At the left of this new gap, α jumps up by one, and at the right it jumps down by one. A closeup of the region near the left jump, indicated by the red arrows in 13(b), is shown in 13(c). It shows a similar structure as 13(b), but at a smaller scale. A closeup of the region indicated by the red arrows in 13(c) is shown in 13(d), and again shows a similar structure as in 13(c). Thus, not only does this figure give more detail on the fractal pattern of the gaps, with gap scales ranging from 8×10^{-5} visible in 13(a) to 4×10^{-6} visible in 13(b) to 2×10^{-7} visible in 13(c), to 5×10^{-8} visible in 13(d), but it also indicates that the gaps within gaps within gaps appear in a self-similar pattern.

The fractal, self-similar nature in which both α and τ jump apparently *ad infinitum* across gaps within gaps indicates the existence of angles β_i^* for which α, τ are arbitrarily large. The existence of such angles is reflected numerically by the large values of α, τ observed in the gaps. In view of the self-similar fractal complexity, these trapping angles are not attained in any limit. That is, it is not true that as β approaches β_i^* the corresponding winding numbers α approach ∞. This makes it harder to find the values of β_i^* numerically. However, their existence can be deduced from the fractal structure revealed. The gaps thus represent trapping regions: regions containing angles for which the vortices do not leave the plate for arbitrarily large times.

As indicated by the results shown so far, the number of trapping regions increases as D/L decreases. The dependence on D/L is shown in Fig. 14, which plots the position of gaps across which α jumps by one, each one representing a trapping region containing the complex behavior described above. For each D/L, the position β_i^c of the center of the gaps is shown. Note that only gaps that are not within gaps already accounted for are shown. For example, for $D/L = 0.25\pi/4$, only the four gaps visible in Fig. 10(a) are shown, and not the many gaps within them. Also, only gaps sufficiently far from gaps already accounted for are plotted. For example, for $D/L = 0.167\pi/4$,

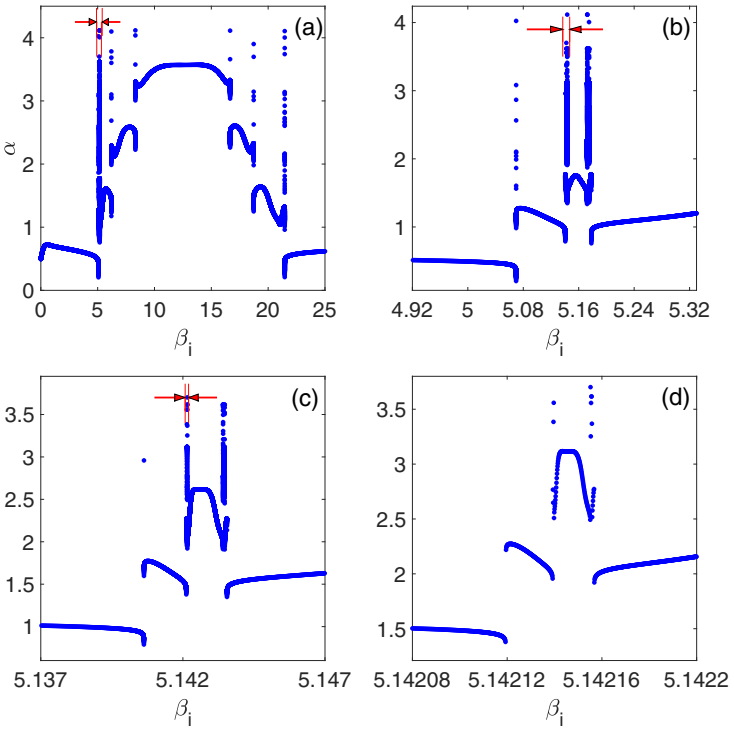

FIG. 13. Winding number α for $D/L = 0.167\pi/4$, vs β_i. Panels (b)–(d) show closeups of the region whose width is indicated by arrows in panels (a)–(c).

only the six gaps visible in Fig. 13(a) and the two additional gaps visible in the closeup in Fig. 13(b) are shown, not the additional gaps visible in Figs. 13(c) and 13(d).

Figure 14(a) shows that for $D/L > 0.471\pi/4$, there are no trapping events for any value of β_i, as observed in Figs. 9(a) and 9(b). For $0.303\pi/4 < D/L \leqslant 0.471\pi/4$, there are two trapping, as in Fig. 9(c). For $0.218\pi/4 < D/L/(\pi/4) \leqslant 0.303\pi/4$, there are four, as in Fig. 9(d). For $0.159\pi/4 < D/L \leqslant 0.218\pi/4$, there are six major branches as in Fig. 13(a), and for $0.15\pi/4 \leqslant D/L \leqslant 0.159\pi/4$, there are eight major branches. The closeups in Figs. 14(b) and 14(c) show the emergence of new branches near existing branches, corresponding to the branches observed in Fig. 13(b). Figure 14 thus shows the increasing appearance of trapping regions as D/L increases. It also shows that, near the critical angles, the dependence of the trajectories is highly singular under changes both in β_i or D/L.

The observed scattering and trapping of the vortex dipoles is reminiscent of the dynamics observed in Ref. [16] for the interaction of pairs of dipoles in unbounded flows, although the scattering is not resolved there in as much detail as here. It is expected that the observed behavior is stable to perturbations, with continuous perturbations of the upstream starting position yielding similar bifurcation diagrams as that in Fig. 14.

C. Separation of incoming sequence of dipoles by an oscillating plate

We now apply the observed sensitivity of the transmitted angle to changes in the incident angle to separate an incoming sequence of vortex dipoles by oscillating the plate. Consider a sequence of dipoles added at periodic time intervals at one point in the x-y plane, as if, for example, a sequence of planes were flying along the same path, normal to the x-y plane, each generating a trailing vortex dipole. The wake hazard caused by vortices of a preceding aircraft on a following aircraft is one of

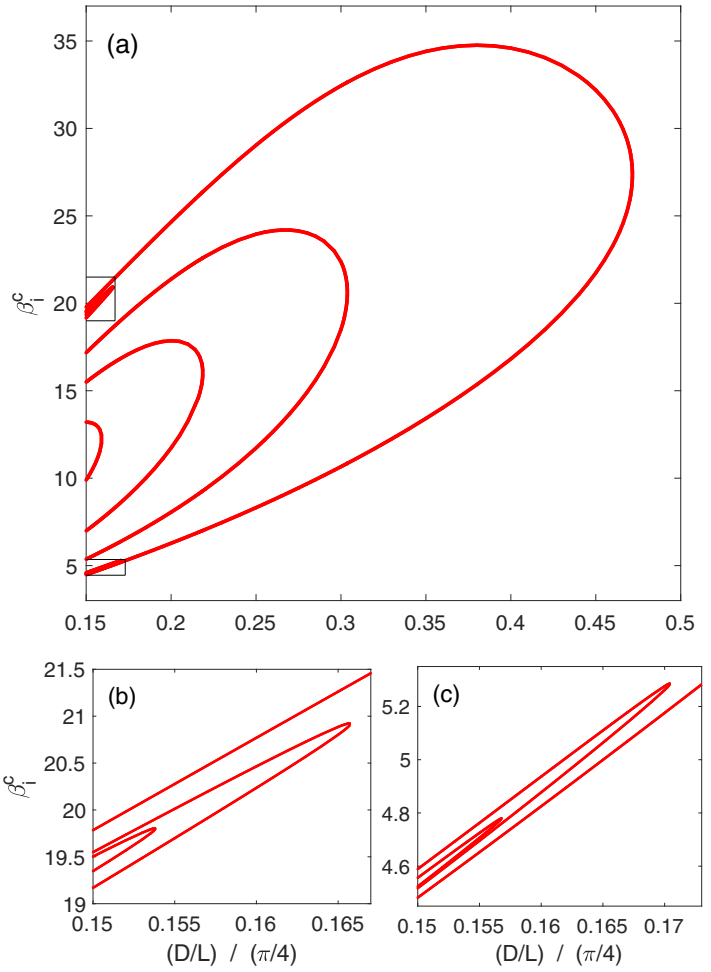

FIG. 14. Diagram showing the position of trapping regions centered at β_i^c, as a function of D/L. Panels (b) and (c) are closeups of the boxed regions in panel (a).

the main reasons limiting the time between take-off and landing at airfields. The ability to deflect and separate a sequence of vortices could potentially be useful in remediating the wake hazard. This section addresses a highly idealized situation.

A sequence of counter-rotating vortex pairs is added to the flow at a fixed position $(\pm D/L,3)$, at periodic time intervals τ_v. A plate is placed at the origin in the path of the vortices, but instead of being stationary, it oscillates about the vertical with period τ_p, amplitude β_M, and phase shift ϕ, with

$$\beta_i(t) = \beta_M \cos\left(\frac{2\pi(t-\phi)}{\tau_p}\right). \tag{12}$$

The simulations shown in this section are obtained with sample values of $\beta_M = 20^\circ$, $\tau_p = 40$, and $\phi = 12$, with $D/L = \pi/4$. The value of ϕ determines at what plate position the vortices reach the vicinity of the plate and is chosen so as to maximize the resulting deflection.

Consider the case with $2\tau_v = 3\tau_p$. A dipole is inserted at times $t = 0,\tau_v,2\tau_v,3\tau_v,\ldots = 0,1.5\tau_p,3\tau_p,\ldots$. Since the plate oscillates with period τ_p, after an interval of $3\tau_p$, the plate and

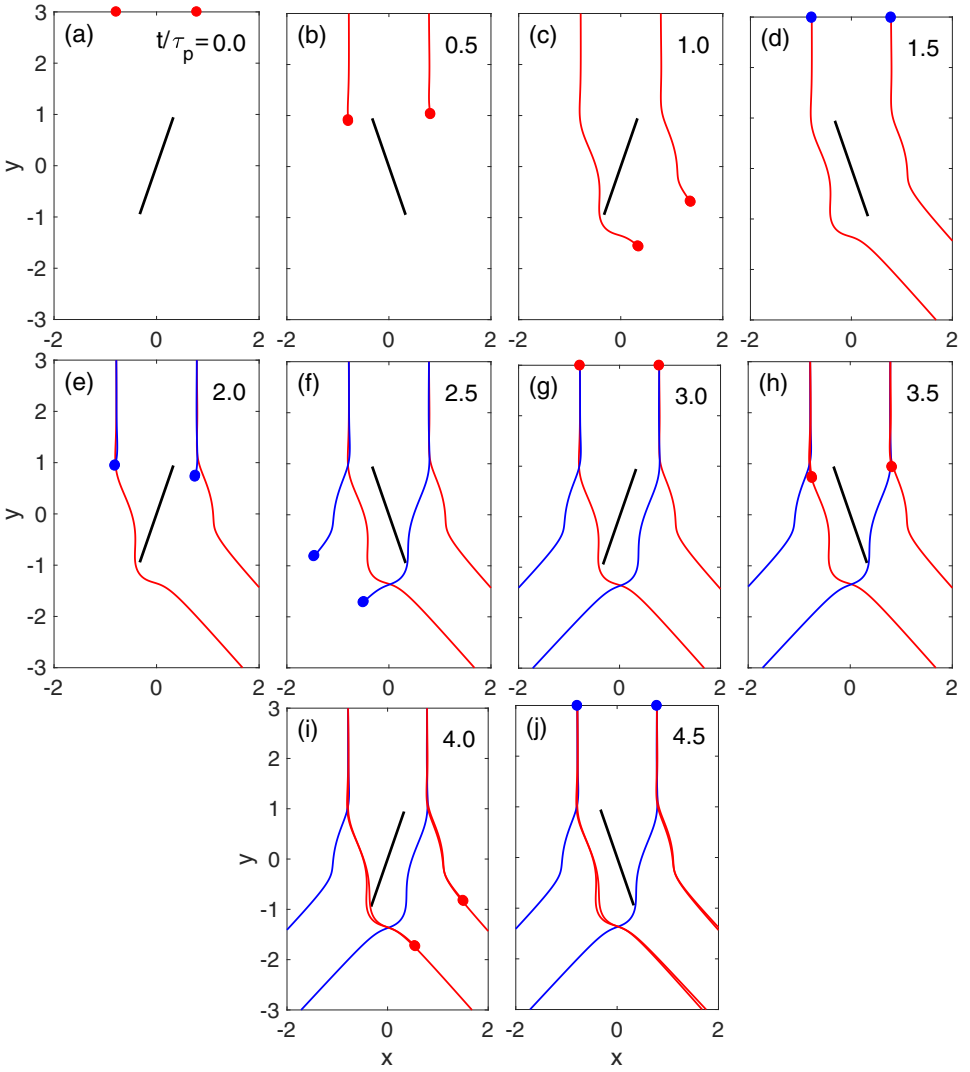

FIG. 15. The plate oscillates with period $\tau_p = 40$. Dipoles are inserted at $y = 3$ at time intervals τ_v with $2\tau_v = 3\tau_p$. The position of all vortices is shown at the indicated times t/τ_p (solid dots), with all previous trajectories shown as curves.

incoming dipole are in the same relative position as at the beginning of the interval. The dipole-plate position thus repeats itself periodically with period $3\tau_p$. In that interval two dipoles have entered the flow at different phases of the plate and thus take two different paths. Afterward the flow repeats itself almost periodically. This is illustrated in Fig. 15. The figure shows the plate position and the dipole positions at the indicated times t/τ_p. The dipole positions are shown as solid dots. The attached curves show the traversed dipole trajectory. In frame 15(a), a dipole is inserted at the top of the figure, $y = 3$, at $t = 0$. Its later trajectory is seen as the red curve in all later frames. In frame 15(c), it is deflected by the plate to the right. In frame 15(d), a second dipole is inserted at the top of the figure, at $t = \tau_v = 1.5\tau_p$. Its later trajectory is seen as the blue curve in all later frames. In frame 15(e), it approaches the plate at a different phase than the first vortex in frame 15(b), and as a result it moves on a different trajectory. In frame 15(f), it is deflected to the left instead of the right. A third

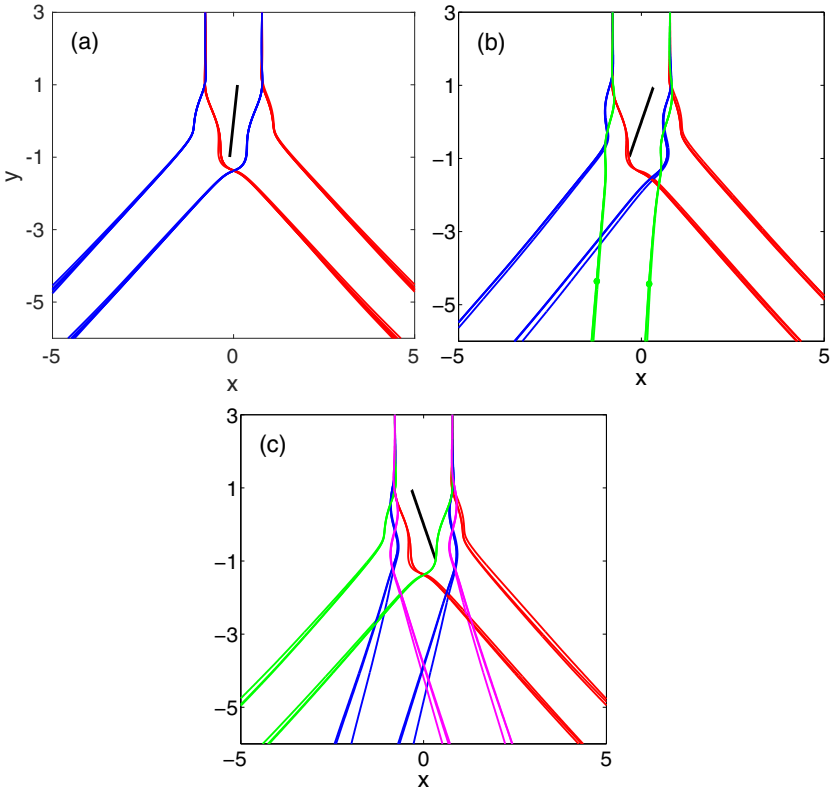

FIG. 16. Trajectories of the first 12 dipoles inserted at $y = 3$ at time intervals τ_v, where (a) $2\tau_v = 3\tau_p$, (b) $3\tau_v = 5\tau_v$, (c) $4\tau_v = 7\tau_v$. In all cases, the plate oscillation period is $\tau_p = 40$.

dipole is inserted at $t = 2\tau_v = 3\tau_p$ in frame 15(g). Frames 15(i) and 15(j) show that its trajectory is almost superposed to the one of the first dipole.

Further dipoles are introduced at the same interval $\tau_v/\tau_p = 3/2$. Figure 16(a) shows the resulting paths of the first 12 dipoles. The trajectories are clearly separated into two paths. The motion is not completely periodic since each dipole does not have the same number of dipoles behind it. This is most noticeable for the first dipole, whose track is slightly different than that of the following ones.

This result yields a procedure to separate a sequence of dipoles into an arbitrary number of paths. If $n\tau_v = m\tau_p$ and n,m are relatively prime, with n smaller than m, then after $t = m\tau_p$ the process will first repeat itself and the incoming dipoles will be separated into n paths. Figures 16(b) and 16(c) show the resulting paths of the first 12 dipoles with $3\tau_v = 5\tau_p$ and $4\tau_v = 7\tau_p$, respectively.

V. SUMMARY AND REMARKS

Numerical simulations were presented of an apparently simple problem of a counter-rotating vortex pair interacting with a plate in its path. In all computed cases, the vortex pair leaves the plate eventually, after some time delay, as a dipole with unchanged velocity but generally large changes in direction. The plate deflects the dipole to the left or to the right, at transmitted angles that depend sensitively on the incident angle. The sensitivity, measured by the derivative $d\beta_t/d\beta_i$, increases rapidly as the plate length L increases relative to the vortex size D. For sufficiently small $D/L < 0.471\pi/4$, singular events occur near critical incident angles. In these regions, infinitesimal changes in β_i or D/L lead to abrupt and discontinuous changes in the topology of the dipole trajectory. The singularities are evident as jumps in the winding number α of one vortex about the

plate and in the time delay τ as β_i changes across an interval. Within these intervals, jumps occur in a self-similar fractal fashion, indicating the existence of incident angles that delay the dipole motion indefinitely, thus trapping the vortices near the plate. The number of such intervals, referred to as trapping regions, and the complexity of the dependence on β_i and D/L increases as D/L decreases. The simulations thus show that, even for an apparently simple setup, the dynamics of a two-point-vortex system interacting with a wall is surprisingly rich. The sensitivity was applied to separate an incoming stream of dipoles by oscillating the plate.

Point vortex dynamics are of interest in their own sake, but also to yield insight into physical vortex dynamics, in which generally viscosity does not permit slip past walls. One question the present work raises is to what extent the behavior observed here is reflected in viscous flow. Careful laboratory experiments or viscous simulations, beyond the scope of this work, are necessary to obtain further insight into using plates to control vortical flows.

ACKNOWLEDGMENTS

I thank Robert Krasny, Patrick Weidman, and the anonymous referees for many valuable comments and suggestions.

APPENDIX: MOTION OF A SINGLE VORTEX PAST A PLATE

Figures 1(c) and 1(d) briefly addressed the motion of a single vortex past a plate with zero circulation. This appendix describes the single vortex trajectory in more detail, to better understand its regularity and its dependence on the distance of the vortex from the plate. We consider a single point vortex positioned near a flat plate, in otherwise irrotational inviscid flow that vanishes at infinity. The plate lies horizontally on the line $\{(x,0)| -1 \leqslant x \leqslant 1\}$ and the vortex is initially positioned at a distance ϵ above the plate, at $(0,\epsilon)$. The flow is normalized by the plate half-length and the vortex circulation, as in the rest of this paper. Figure 17(a) plots the trajectory of the vortex, for four values of $\epsilon = 0.2, 0.1, 0.05, 0.025$. The initial position in each case is indicated by the solid dot. In each case, the vortex, with positive circulation $\Gamma = 1$, rotates clockwise around the plate. The smaller ϵ is, the more parallel is the trajectory along the plate. The closeup in Fig. 17(b) shows that, even near the edge, the vortex trajectory remains regular and smooth for any value of ϵ. For smaller ϵ, it turns more tightly around the edges, in shape close to a half-circle with radius proportional to ϵ. The shapes are similar to much of the trajectory of the right vortex shown in Fig. 7.

The time that a single vortex takes for a full rotation about the plate, denoted by T, is shown in Fig. 18. The figure plots T/ϵ for a range of values of ϵ, and shows that T scales like ϵ as $\epsilon \to 0$, with

$$T = C_\epsilon \epsilon \text{ where } \lim_{\epsilon \to 0} C_\epsilon \approx 50.2655. \tag{A1}$$

That is, the closer the vortex is to the plate, the faster it moves around it, as expected.

Figure 19(a) plots the speed of the vortex over one period vs time scaled by the total period T. The speed is scaled by $1/\epsilon$. It shows that $|\mathbf{u}|$, as expected, remains proportional to $1/\epsilon$ throughout. Moreover, the speed around the edges, which the vortex approaches at $t/T = 0.25, 0.75$, is never significantly larger than the vortex speed along the sides of the plate. In fact, the maximal speed around the edges is approximately twice the vortex speed along the sides, for all $\epsilon > 0$. The speed increases from approximately $0.08/\epsilon$ to about $0.16/\epsilon$ in a time interval of size proportional to ϵ. This is shown in Fig. 19(b), which plots the scaled velocity about the right edge, where $t/T = 0.25$, vs time from the edge scaled by $1/\epsilon$. With this scaling, the curves for all four values of ϵ collapse onto one.

Finally, we note that although the vortex motion and speed remain regular for all $\epsilon > 0$, the flow near the edges of the plate is not regular, since the Kutta condition is not satisfied. The vortex induces a flow near the plate of magnitude Γ/ϵ, which in turn induces singular flow at the plate tip of order $1/\sqrt{x}$ where x is the distance from tip. However, although the fluid about each of the plate edges is singular, the vortex motion remains regular.

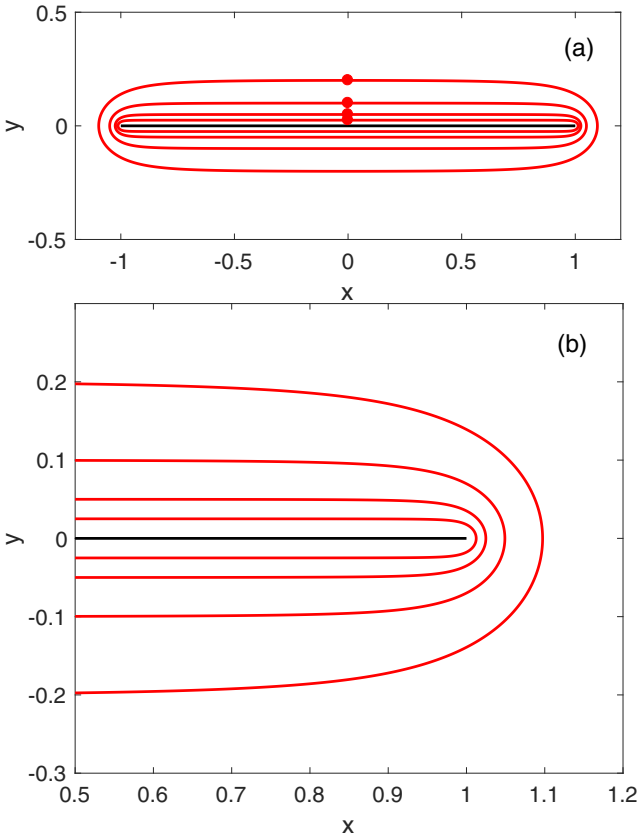

FIG. 17. Trajectories of single vortices moving near a plate in otherwise inviscid, irrotational flow with vanishing velocity at ∞. The dots denote the initial vortex position at $(0,\epsilon)$, for $\epsilon = 0.2, 0.1, 0.05, 0.025$. The vortices rotate clockwise around the plate. Panel (b) shows a closeup of panel (a) near the right plate edge.

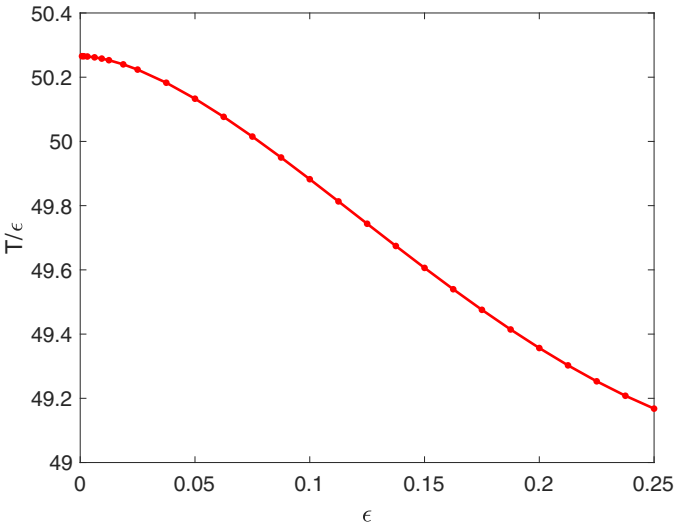

FIG. 18. Time T taken by a single vortex for one rotation around the plate, scaled by ϵ, vs ϵ, where ϵ is the initial vortex distance from the plate.

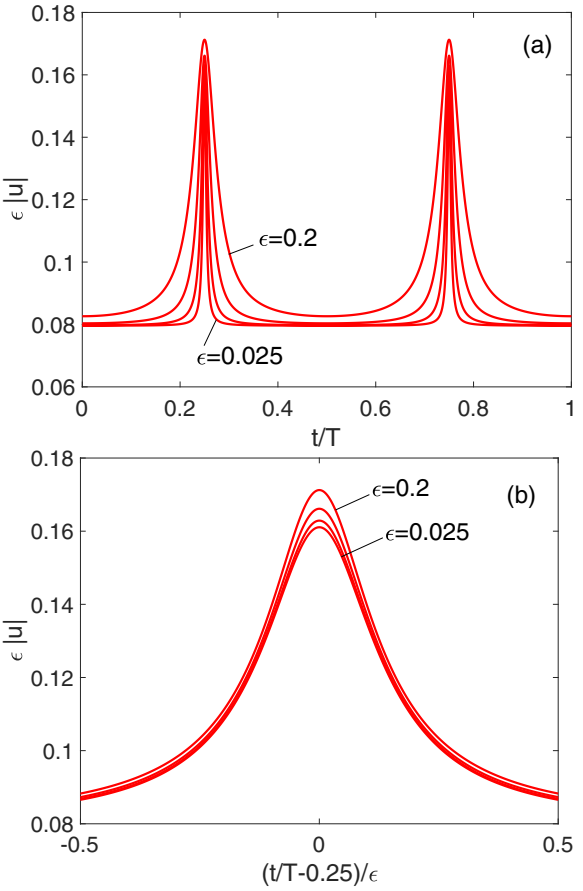

FIG. 19. Vortex speed, scaled by $1/\epsilon$, vs (a) normalized time t and (b) a scaled normalized time near the right edge, at which $t/T = 0.25$. Results are shown for $\epsilon = 0.2, 0.1, 0.05, 0.025$.

In the simulations presented in this paper, the right vortex behaves as a single vortex near the plate for much of the time, especially in the singular regime where winding numbers are high. However, in all runs, the maximum vortex speed is always less than eight. Since according to Fig. 19, $0.08 < \epsilon|u| < 0.17$, it follows that the vortices in all calculations presented in Secs. IV A and IV B stay at a distance $>0.08/8 = 0.01$ units from the plate.

[1] P. K. Newton, *The N-Vortex Problem* (Springer Verlag, New York, 2001).
[2] H. Aref, Point vortex dynamics: A classical mathematical playground, J. Math. Phys. **48**, 065401 (2007).
[3] H. Aref, Stability of relative equilibria of three vortices, Phys. Fluids **21**, 094101 (2009).
[4] P. Beelen, M. Brøns, V. S. Krishnamurthy, and M. A. Stremler, Recent progress in the relative equilibria of point vortices—In memoriam Hassan Aref, Procedia IUTAM **7**, 3 (2013).
[5] E. R. Johnson and R. N. McDonald, The motion of a vortex near two circular cylinders, Proc. R. Soc. London, Ser. A **460**, 939 (2004).
[6] E. R. Johnson and R. N. McDonald, The motion of a vortex near a gap in a wall, Phys. Fluids **16**, 462 (2004).

[7] E. R. Johnson and R. N. McDonald, Vortices near barriers with multiple gaps, J. Fluid Mech. **531**, 335 (2005).
[8] D. Crowdy and J. Marshall, On the motion of a point vortex around multiple circular islands, Phys. Fluids **17**, 056602 (2005).
[9] D. Crowdy and J. Marshall, The motion of a point vortex through gaps in walls, J. Fluid Mech. **551**, 31 (2006).
[10] A. Surana D. G. Crowdy and K.-Y. Yick, The irrotational flow generated by two planar stirrers in inviscid fluid, Phys. Fluids **19**, 018103 (2007).
[11] P. G. Saffman and J. S. Sheffield, Flow over a wing with an attached free vortex, Stud. Appl. Math. **57**(2), 107 (1977).
[12] M. G. Wells and G.-J. F. van Heijst, A model of tidal flushing of an estuary by dipole formation, Dynam. Atmos. Ocean **37**(3), 223 (2003).
[13] P. K. Newton and H. Shokraneh, Interacting dipole pairs on a rotating sphere, Proc. R. Soc. London, Ser. A **464**, 1525 (2008).
[14] J. Archer, Deflection of an elliptically loaded vortex sheet by a flat plate, Rose-Hulman Undergraduate Mathematics Journal **15**(1), 107 (2014).
[15] R. Krasny, Computation of vortex sheet roll-up in the Trefftz plane, J. Fluid Mech. **184**, 123 (1987).
[16] B. Eckhardt and H. Aref, Integrable and chaotic motions of four vortices ii. Collision dynamics of vortex pairs, Philos. Trans. R. Soc. A **326**, 655 (1988).
[17] M. Nitsche and R. Krasny, A numerical study of vortex ring formation at the edge of a circular tube, J. Fluid Mech. **276**, 139 (1994).
[18] P. G. Saffman, *Vortex Dynamics* (Cambridge University Press, Cambridge, 1992).